ARTICLE

The molecular structure of the surface of water-ethanol mixtures

Johannes Kirschner,*[a] Anderson H. A. Gomes,[b,1] Ricardo R. T. Marinho,[c] Olle Björneholm,[d] Hans Ågren,[d,e] Vincenzo Carravetta,[f] Niklas Ottosson,[g,2] Arnaldo Naves de Brito[b] and Huib J. Bakker[a]

Received 00th January 20xx,
Accepted 00th January 20xx

DOI: 10.1039/x0xx00000x

Mixtures of water and alcohol exhibit an excess surface concentration of alcohol as a result of the amphiphilic nature of the alcohol molecule, which has important consequences for the physico-chemical properties of water-alcohol mixtures. Here we use a combination of intensity vibrational sum-frequency generation (VSFG) spectroscopy, heterodyne-detected VSFG (HD-VSFG), and core-level photoelectron spectroscopy (PES) to investigate the molecular properties of water-ethanol mixtures at the air-liquid interface. We find that increasing the ethanol concentration up to a molar fraction (MF) of 0.1 leads to a steep increase of the surface density of the ethanol molecules, and an increased ordering of the ethanol molecules at the surface. When the ethanol concentration is further increased, the surface density of ethanol remains more or less constant, while the orientation of the ethanol molecules become increasingly disordered. The used techniques of PES and VSFG provide complementary information on the density and orientation of ethanol molecules at the surface of water, thus providing new information on the molecular-scale properties of the surface of water-alcohol mixtures over a wide range of compositions. This information is invaluable in understanding the chemical and physical properties of water-alcohol mixtures.

Introduction

Many chemical reactions take place at liquid water-air interfaces, and detailed knowledge of the molecular structure of aqueous surfaces is crucial for the understanding of the mechanism and kinetics of such reactions. Previous theoretical and experimental studies revealed that the molecular surface structure of aqueous solutions often differ substantially from that of the bulk.[1] An intrinsic difficulty in experimentally studying surface properties is that in most techniques the signal of the molecules in the surface layers is completely overwhelmed by the signal of the bulk. Over the last decades, this difficulty has been overcome with the development of new surface-specific techniques suitable for studying liquid interfaces. One of these techniques is surface sum-frequency generation (SFG) which owes its high surface specificity from the fact that the process of sum-frequency generation is forbidden for systems possessing inversion symmetry, which is the case for most bulk liquids.[2–5] SFG has been widely applied to study the properties of molecular adsorption of water-alcohol mixtures at liquid/solid interfaces.[6,7] Another surface-specific technique is photoelectron spectroscopy in which the surface specificity results from the limited inelastic mean free path (IMFP) of the ejected electrons upon photoionization. The IMFP is energy dependent and for most condensed materials it has a minimum value of near 1 nanometer around 100 electron volts (eV) of kinetic energy. As a result, only electrons near the surface can escape from the sample and can reach the detector.

For liquid mixtures an important question is how the molecules of the different components are distributed over the bulk and the surface, since many chemical reactions and interactions occur at the surface, and the reactivity is often strongly dependent on the local concentration, e.g. the concentration at the surface. It is conceivable that the different components of the mixture show an entirely different surface propensity, even in naturally abundant mixtures and biologically important mixtures of water and amphiphilic compounds. These effects can be well studied in mixtures of water and small alcohols like ethanol, as the composition of these mixtures can be varied over the whole range between the limits of pure alcohol and pure water.

Mixtures of water and different alcohols have previously been studied with a variety of experimental and theoretical approaches, often arriving at different conclusions regarding the surface structure and composition, because the obtained data are often not exclusively representing the response of the

[a] *Ultrafast Spectroscopy, AMOLF, 1098 XG Science Park, Amsterdam, The Netherlands*
[b] *Dept. of Applied Physics, Institute of Physics "Gleb Wataghin", University of Campinas, CEP: 13083-859 Campinas-SP, Brazil*
[c] *Institute of Physics, Federal University of Bahia, 40.170-115, Salvador, BA, Brazil*
[d] *Department of Physics and Astronomy, Uppsala University, 752 36 Uppsala, Sweden*
[e] *Theoretical Chemistry and Biology, School of Chemistry, Biotechnology and Health, KTH Royal Institute of Technology, SE-10044 Stockholm, Sweden*
[f] *CNR-IPCF, Institute of Chemical and Physical Processes, via G.Moruzzi 1, I-56124 Pisa, Italy*
[g] *EUV Photoemission, ARCNL, 1098 XG Science Park, Amsterdam, The Netherlands*
[1] Current address: Laboratório Nacionalde Luz Síncrotron (LNLS)",13084-971 Campinas-SP, Brazil
[2] Current address: Swedish Research Council, Västra Järnvägsgatan 3, 111 64 Stockholm
Supplementary Information (SI) available: See DOI: 10.1039/x0xx00000x

surface, and because the observed data and trends can have different molecular-scale explanations.[8–14] For instance, a decrease in signal can be due to a decrease of the surface density of the probed molecular species, but also due to a change of the average orientation or an increased orientational disorder of the probed molecules.[8–14]
Many of these studies include investigations of the surface of water-alcohol mixtures with vibrational sum-frequency generation (VSFG).[15–22] Up to now mainly intensity VSFG measurements provided important information on the nature and density of the molecules at the surface, but limited information on the orientation of these molecules. Here we study the surface of water-ethanol mixtures with heterodyne-detected VSFG, which provides detailed information on the molecular orientation of the surface molecules. The combination of this technique with conventional intensity VSFG and photoelectron spectroscopy allows for the first unambiguous determination of the surface density and orientation of the ethanol molecules at the surface over a wide range of ethanol-water mixture compositions.

Experimental

We study the surface structure of mixtures of water and ethanol throughout the whole concentration range (0% to 100% molar fraction (MF) bulk concentration), with vibrational surface sum-frequency generation (VSFG) and photoelectron spectroscopy (PES) (0%-85%). In the VSFG experiments, we measure the signals of the vibrations of the methyl (CH3) group of ethanol and the OH stretch vibration of the OH groups of water molecules that are sticking out of the surface. The latter signal turns out to be a useful probe for the surface coverage of ethanol molecules at low concentrations. In the PES experiments, we detect the carbon 1s core-level photoemission signals from both carbon sites.

Sample preparation

The ethanol used in both spectroscopic experiments was purchased from Sigma Aldrich and had a purity exceeding 99.9%. The ethanol was used without further purification. We prepared ethanol/water mixtures by adding Millipore water (18.2 MΩ cm at 25˚C). We varied the ethanol molar fraction from 0.1% MF (0.001 MF) to 100% MF (1.0 MF). The samples were used on the day of preparation and kept in a closed sample cell to avoid evaporation. The SFG measurements were carried out at room temperature (23 °C). The PES experiments were performed at a temperature of ~10 °C using a jet flow of ~0.5 mL/min.

VSFG experiment

The details of our VSFG setup have been described before.[23] Briefly, a Ti:Sapphire regenerative amplified laser system with a repetition rate of 1 kHz produces 35 femtosecond pulses with a wavelength of 800 nm. The output of this laser is split in two parts. One part is used in a home-built optical parametric amplifier (OPA) to produce a tuneable broad-band infrared pulse. The second part of the 800 nm beam is spectrally narrowed using an etalon, and subsequently temporally and spatially overlapped with the broad-band infrared pulse at the sample surface to generate the sum-frequency signal (see Figure 1a). The SFG signal is sent into a monochromator and detected with a CCD camera (EMCCD from Andor Technologies).

To obtain information about the orientation of the stretch vibrations, we use heterodyne detected VSFG (HD-VSFG).[24] In this technique, we first generate an SFG signal at the surface of a gold mirror that serves as a local oscillator (LO-SFG). The IR and VIS beams are reflected from this mirror and are focused together with the LO-SFG signal on the sample. The LO-SFG signal is delayed in time using a silica plate. The IR and VIS beams generate a VSFG signal at the sample. This sample VSFG signal and the LO-SFG signal that is reflected from the sample are both sent into a monochromator and detected by a CCD camera. The interference of the two signals leads to a modulated spectrum. A schematic sketch of the HD-SFG signal generation is shown in Figure 1b. After Fourier transformation, filtering, and back Fourier transformation, we obtain an HD-SFG spectrum that is the product of the LO-SFG and the sample VSFG electric fields.

To correct the measured data for the spectral shape of the IR pulse, we replace the sample by a z-cut α-quartz crystal, and we measure a reference HD-SFG spectrum. Subsequently, we divide the HD-VSFG spectrum of the sample by the reference HD-SFG spectrum, which yields the frequency-dependent second-order susceptibility $\chi^{(2)}$. The spectral shape and sign of $\chi^{(2)}$ contain relevant information on the nature of the molecular groups and their orientation at the surface.

a)

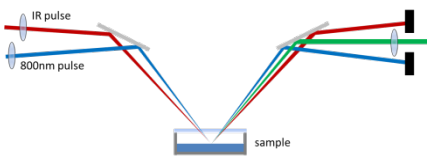

b)

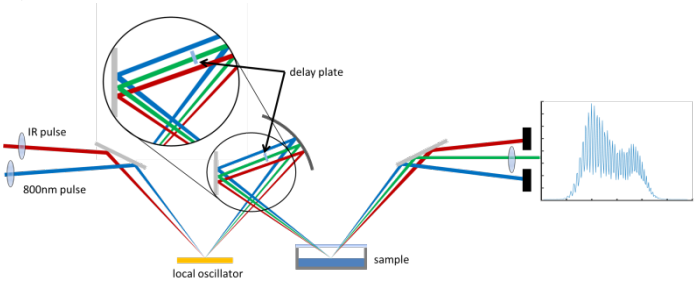

Figure 1: Schematic drawing of the a) intensity VSFG and b) the heterodyne detected VSFG setup.

VSFG theory

The signal measured by HD-VSFG depends on the second order susceptibility $\chi^{(2)}$, which is a third rank tensor and has therefore 27 elements. Due to symmetry consideration, the surface of centrosymmetric systems has only seven non-zero $\chi^{(2)}$ tensor elements: $\chi^{(2)}_{xxz} = \chi^{(2)}_{yyz}$, $\chi^{(2)}_{xzx} = \chi^{(2)}_{yzy}$, $\chi^{(2)}_{zxx} = \chi^{(2)}_{zyy}$ and $\chi^{(2)}_{zzz}$. In VSFG we measure an effective second-order susceptibility $\chi^{(2)}_{eff}$ of which the value depends on the $\chi^{(2)}$ tensor elements, the polarization configuration, and the Fresnel coefficients L_{ii} [25–27]:

SSP:

$$\chi^{(2)}_{eff,ssp} = L_{yy}(\omega_{SF})L_{yy}(\omega_{VIS})L_{zz}(\omega_{IR})\,sin(\eta_{IR})\,\chi^{(2)}_{xxz} \quad (1)$$

PPP:

$$\begin{aligned}\chi^{(2)}_{eff,ppp} = &-L_{xx}(\omega_{SF})L_{xx}(\omega_{VIS})L_{zz}(\omega_{IR})\cos(\eta_{SF})\cos(\eta_{VIS})\sin(\eta_{IR})\,\chi^{(2)}_{xxz}\\ &- L_{xx}(\omega_{SF})L_{zz}(\omega_{VIS})L_{xx}(\omega_{IR})\cos(\eta_{SF})\sin(\eta_{VIS})\cos(\eta_{IR})\,\chi^{(2)}_{xzx}\\ &+ L_{zz}(\omega_{SF})L_{xx}(\omega_{VIS})L_{xx}(\omega_{IR})\sin(\eta_{SF})\cos(\eta_{VIS})\cos(\eta_{IR})\,\chi^{(2)}_{zxx}\\ &+ L_{zz}(\omega_{SF})L_{zz}(\omega_{VIS})L_{zz}(\omega_{IR})\sin(\eta_{SF})\sin(\eta_{VIS})\sin(\eta_{IR})\,\chi^{(2)}_{zzz}\end{aligned} \quad (2)$$

In these equations $\eta_{IR,VIS}$ denotes the incident angles of the IR and VIS beams and η_{SF} the reflecting angle of the SF signal, respectively, and the subscripts s and p denote the polarization of the SFG, the visible and the IR beam. The subscript ssp means that the SFG light is s-polarized, the visible light is s-polarized, and the IR beam is p-polarized.
The signal measured with a polarization combination SSP thus represents only tensor element $\chi^{(2)}_{xxz}$, while the signal measured with polarization combination PPP combination depends on all four independent tensor elements. The tensor elements depend on the molecular hyperpolarizabilities and the orientation of the molecular vibration being probed.

PES experiment

The PES experiment was performed using an electron spectrometer at the I1011/I411 undulator beamline at the MAX-lab synchrotron facility, Lund, Sweden [28,29]. Using a photon energy of 360 eV, the C1s photoelectrons have a kinetic energy of approximately 70 eV, resulting in an attenuation length of 0.5−1 nm [30–32]. For these experiments we used a liquid jet setup, see Figure 2, provided by Microliquids GmbH. Details on this technique can be found elsewhere [33–36]. Briefly it consists of a thin 18−20 µm jet ejected through a nozzle into the vacuum chamber. At the interaction point, the jet is intersected by the x-rays in front of a skimmer, which forms part of a differential pumping stage protecting the rest of the setup, requiring ultra-high vacuum, from the relatively high pressure around the liquid jet (determined by the vapour pressure of the sample). The photoionization was performed with linearly polarized synchrotron light that overlaps with the microjet about 1 mm after the injection point and well before the liquid jet breaks up into droplets and eventually freezes. A hemispherical electron analyzer (Scienta R4000) mounted in the magical angle relative to the polarization plane of the synchrotron light detects the photoelectrons. By doing so, photoelectron angular distribution effects are minimized [37]. The total experimental resolution is around 0.3 eV, as determined from the width of the water gas phase valence band $1b_1$ state. Therefore, this broadening is substantially less than the inherent width of the peaks from the liquid sample. All spectra were energy calibrated against the binding energy of the $1b_1$ state of liquid water, with a binding energy of 11.16 eV [38], and intensity-normalized against photon flux and acquisition time. In order to avoid charging of the liquid jet due to electrokinetic charging and photoionization, all solutions contained 25 mM of NaCl.

The synchrotron beam had a diameter of about 1 mm at the interaction point thus, far larger than the beam of the liquid jet. The relatively large size of the X-ray spot compared to the width of the jet makes the setup insensitive to small changes in the relative positioning of the jet and the x-rays, which allowed us to obtain a very stable photoelectron yield when the same sample was measured at different times. The intensity variations were consistently below 5% during the PES experiment. The spectra measured represent a sum of a liquid-phase spectrum from the micro-jet and a gas-phase spectrum from the vapor surrounding the jet. The pure gas-phase spectrum is obtained by lowering the jet until the liquid signal disappears. We notice no difference between runs made before and after each series showing that these spectra represent the gas phase component during a typical series of measurements.

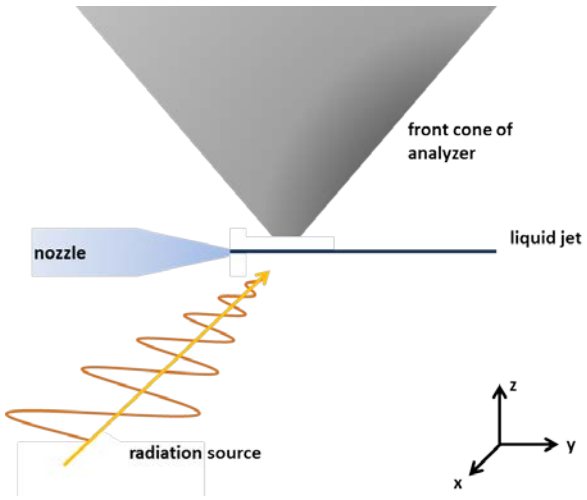

Figure 2: Schematic drawing of the PE setup

We fitted all the PES spectra with Voigt profiles using a least-squares method in IGOR. The lifetime width for C1s core holes corresponding to the Lorentzian width was set to 0.1 eV [39]. The Gaussian widths were free parameters but linked such that they were the same for the corresponding peaks in all spectra. We also allowed the energy positions and intensities to vary freely.

Results and Discussion

Surface density of ethanol

In Figure 3a we present intensity VSFG spectra of binary water-ethanol solutions in the frequency region of the non-hydrogen-bonded OH stretch vibrations (free OH) of water molecules.[40] These free OH groups are mainly present at the surface and therefore constitute a suitable indicator to observe the coverage and shielding of the topmost H_2O molecules of the mixture. We observe that the free OH band has its maximum at a frequency of 3720 cm^{-1}. The amplitude of the free OH peak strongly decreases with increasing concentration of ethanol.

For all spectra we fitted the free OH band with a Lorentzian function (see SI). The fitted area of the free OH band is plotted in Figure 3b as a function of the ethanol molar fraction (MF). It is seen that the area strongly decreases with increasing ethanol concentration, and reaches a constant small value at ~0.1 MF of ethanol. Previous surface tension measurements as a function of ethanol concentration show a very similar trend, which was interpreted as evidence for the formation of a complete monolayer of ethanol at the surface already at low bulk ethanol concentrations.[41,42] The small residual free OH signal can be assigned to non-hydrogen-bonded OH groups of ethanol molecules sticking out of the surface, and to residual uncovered water molecules due to a not perfectly formed monolayer. In Figure 4 we show intensity SFG spectra in the CH range. We assign the peaks at ~2870 cm^{-1} and ~2930 cm^{-1} to mixed bands of the CH_3 symmetric stretch vibration and the overtone of the CH_2 bending mode. These modes have a Fermi resonance and are of strongly mixed character[43,44]. The intensity of these peaks first steeply increases with increasing ethanol concentration, reaching a maximum at a MF of ~0.2. We thus find that at low concentrations the concentration dependence of the amplitude of the CH vibrations is more or less complementary to that of the free OH peak of water. When the concentration of ethanol is further increased, the signal decreases again. This behaviour is also observed for other alcohols like methanol [17,18,41].

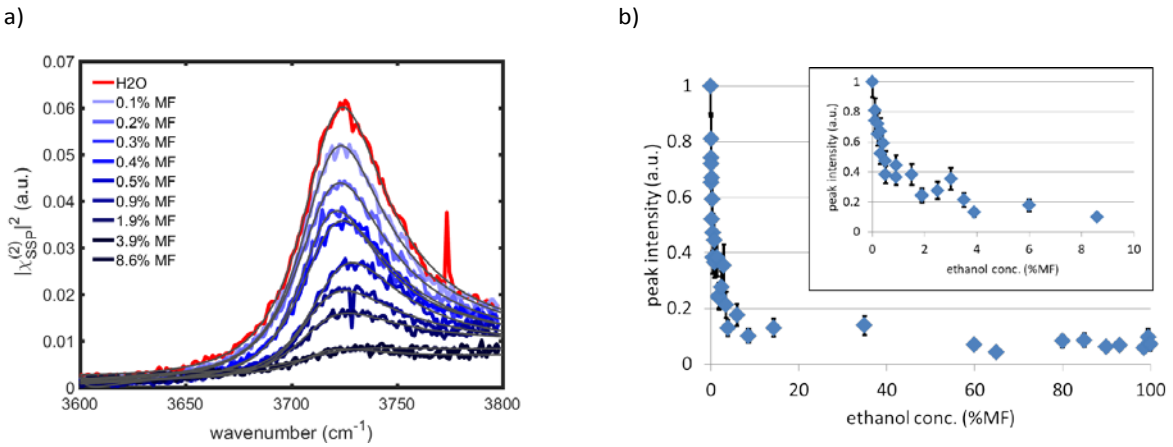

Figure 3: a) SFG intensity spectra for different ethanol concentrations in the free OH region. The grey lines show the fitted spectra. b) Fitted peak intensity of the free OH peak as a function of the ethanol concentration. The inset shows a zoom-in of the plot at low ethanol concentrations (0-10 %MF).

ARTICLE

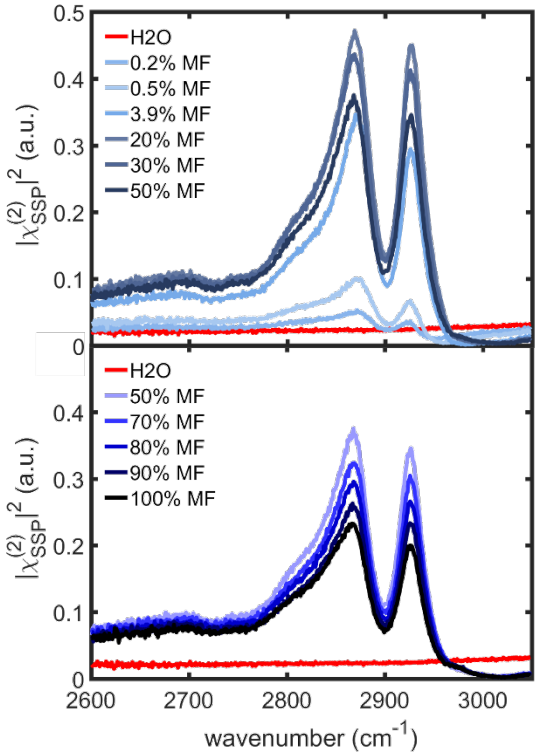

Figure 4: SFG intensity spectra in the CH stretch region.

Several explanations have been offered for this observation including the formation of a double layer with oppositely oriented alcohol molecules, and a decrease of the concentration of alcohol at the surface at high concentrations [17,19–22].

In Figure 5 we present C1s photoelectron spectra of ethanol in the gas phase and of a solution of ethanol in water in a liquid micro-jet. The best fit for the gas-phase peaks was obtained using four asymmetric post-collision interaction (PCI) line profiles. The shape and intensity of the different components are based on a high-resolution spectrum studied and described in detail elsewhere.[45] In Figure 5b we show a typically fitted spectrum containing the gas-phase features together with the liquid-phase components. The shoulder around 290 eV binding energy is assigned to the C1s signal of the CH_3 group in the liquid phase (band in blue), and a second symmetric Voigt line profile at higher binding energy (band in green) is assigned to the C1s signal of the CH_2OH group in the liquid phase. These assignments are supported by a previous PES study of the ethanol/water bulk hydrogen-bonding pattern.[46]

In Figure 6 we present the peak area of the C1s signal as a function of the molar fraction of ethanol. The total signal measured in PES (C1s CH_3 + C1s CH_2OH) depends on the concentration of ethanol at the surface and, to a smaller extent, the concentration of ethanol in the bulk. To distinguish these two contributions we fitted a modified Langmuir model to the measured PES data:

$$N_{C1s} = \frac{N_{S,max}\, x_{bulk}}{x_{bulk} + (1 - x_{bulk}) e^{\Delta G_{Ads}/_{R\,T}}} + N_{bulk,max}\, x_{bulk} \qquad (3)$$

In this equation N_{C1s} is the total C1s photoelectron signal, $N_{bulk,max}$ is the maximum bulk C1s signal of a pure ethanol solution, x_{bulk} is the ethanol molar fraction in bulk and $N_{S,max}$ is the maximum surface intensity of the C1s signal. In this expression, it is assumed that the surface signal increases nonlinearly as a function of the bulk fraction x_{bulk}, due to a favourable surface adsorption energy, whereas the bulk signal increases linearly with the bulk fraction x_{bulk}. The parameters resulting from the fit are: ΔG=-11.5±0.3 kJ/mol, $N_{S,max}$=(3.05±0.07)x10^5, $N_{bulk,max}$=(2.4±0.2)x10^5. The decomposition of the PES signal in a bulk contribution and a pure surface contribution is presented in Figure 6.

Figure 6 also contains the VSFG SSP intensity as function of bulk ethanol concentration. At low ethanol concentrations, the PES and SFG measurements yield a highly similar steep increase in signal with increasing ethanol concentration, which can be well explained from the substantial increase of the surface density of ethanol. At around 20% MF the signal trends start to differ. The total (bulk + surface) PES signal shows an ongoing increase whereas the VSFG signal reaches a maximum and starts to decrease. This latter observation reflects the fact that the VSFG signal is not only dependent on the concentration of the molecules at the surface, but also on their orientation.

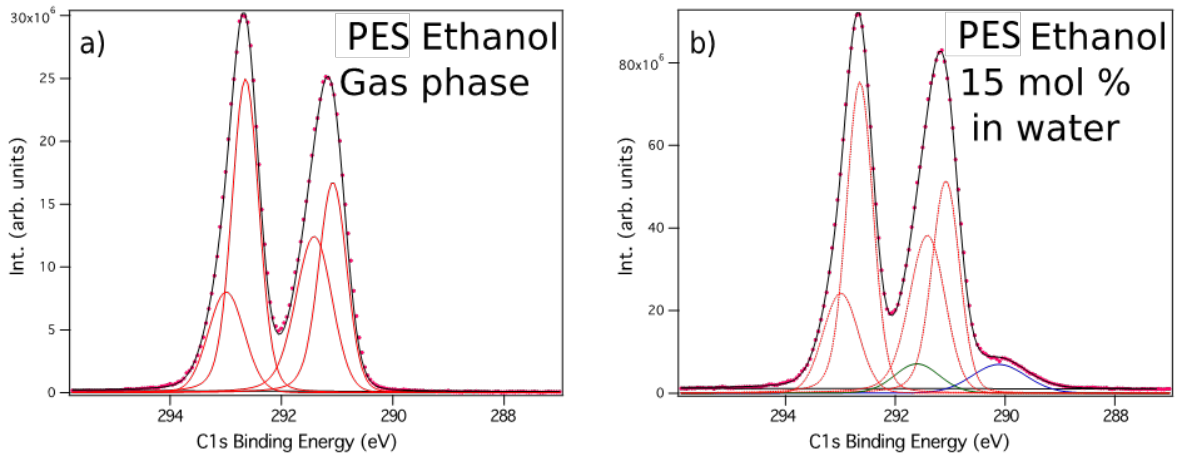

Figure 5: PES C1s spectra of (a) ethanol gas phase taken by lowering the microjet in a way that only vapour overlaps with the X-ray beam (b) a typical C1s PES spectrum from ethanol-water mixtures containing in this case 15 mol% of ethanol. Red dots represent the raw data, red different gas phase vibrational components and solid (b) the liquid phase C1s, CH3 blue and CH2OH green lines are fitted curves (Photon energy = 360 eV). See text for more detail.

Determination of the orientational parameter *D*

In Figure 7 we show HD-VSFG spectra measured with an SSP (a) and a PPP (b) polarization configurations. We observe the mixed bands of the CH_3 symmetric stretch vibration and the overtone of the CH_2 bending mode again. In the PPP spectrum we observe an additional band at 2970 cm^{-1} that we assign to the CH_3 asymmetric stretch vibration. The difference in relative amplitude of the latter mode in the SSP and PPP spectra follows from the fact that SSP and PPP probe different $\chi^{(2)}$ tensor elements [17,18,43,44], as was discussed in the previous section. Similar to the VSFG intensity spectra, the CH bands observed in the HD-VSFG spectra show an initial increase in amplitude with increasing ethanol molar fraction, followed by a decrease when the ethanol concentration exceeds 20% MF (see also Figure 8).

Figure 6: CH_3 ('CH_3 (SFG SSP)') and C1s ('C1s (PES)') peak intensities as a function of the ethanol MF measured with VSFG and PES, respectively. We also show the decomposition of the measured PES signal assuming two regions in which the ethanol density can be different in a bulk contribution and a surface contribution, as described in the text. In the legend 'Fit PES' shows the result of the fit of the Langmuir formula of equation (3) to the total C1s PES intensity, 'PES bulk' is the bulk contribution and 'PES surface' is the surface contribution obtained from this fit.

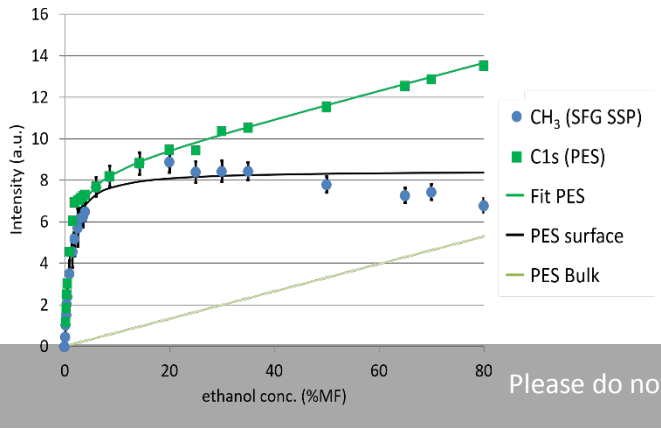

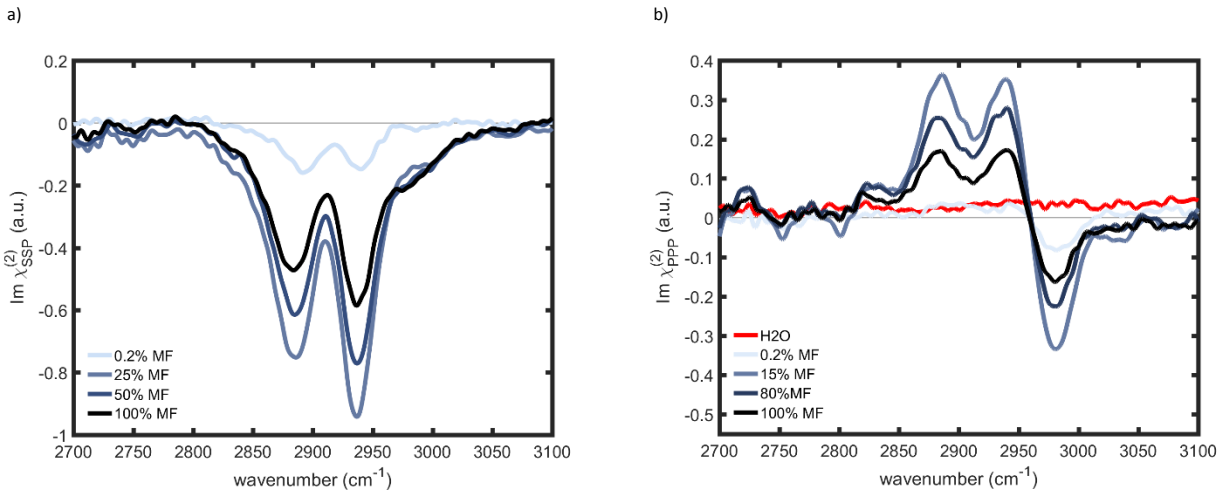

Figure 7: Heterodyne-detected vibrational sum-frequency generation spectra recorded in a) SSP and b) PPP polarizations.

The VSFG signals measured with SSP and PPP polarization combinations depend on Cartesian $\chi^{(2)}$ tensor elements that were introduced in equations (1) and (2). The magnitude of these tensor elements depends on the nature of the vibrations. For the symmetric stretch vibrations, the Cartesian tensor elements are given by:[2,43,47]

$$\chi_{xxz}^{(2),SS} = \frac{1}{2} N_S \beta_{ccc} \langle \cos(\theta) \rangle [(1+R) - (1-R)D] \quad (4)$$

$$\chi_{xzx}^{(2),SS} = \chi_{zxx}^{(2),SS} = \frac{1}{2} N_S \beta_{ccc} (1-R) \langle \cos(\theta) \rangle (1-D) \quad (5)$$

$$\chi_{zzz}^{(2),SS} = N_S \beta_{ccc} \langle \cos(\theta) \rangle [R + (1-R)D] \quad (6)$$

and for the asymmetric vibration by

$$\chi_{xxz}^{(2),AS} = -N_S \beta_{aca} \langle \cos(\theta) \rangle (1-D) \quad (7)$$

$$\chi_{xzx}^{(2),AS} = \chi_{zxx}^{(2),AS} = N_S \beta_{aca} \langle \cos(\theta) \rangle D \quad (8)$$

$$\chi_{zzz}^{(2),AS} = 2N_S \beta_{aca} \langle \cos(\theta) \rangle (1-D) \quad (9)$$

Here, θ is the tilt angle between the methyl group axis and the surface normal, N_S the number of the probed molecules and R the ratio of the hyperpolarizability elements (β_{aac}/β_{ccc}), and D is the orientational parameter ($D = \langle \cos^3\theta \rangle / \langle \cos\theta \rangle$) which gives information about the average orientation and angular distribution. The tensor elements $\chi_{xxz}^{(2)}$, $\chi_{xzx}^{(2)}$, $\chi_{zxx}^{(2)}$ and $\chi_{zzz}^{(2)}$ that enter the expressions for $\chi_{eff,ssp}^{(2)}$ and $\chi_{eff,ppp}^{(2)}$ of equation (1)-(3) are sums of the corresponding tensor elements of the symmetric and asymmetric vibrations. It is clear from the above expressions that all tensor elements scale with $N_S \langle \cos(\theta) \rangle$. Hence, the shapes of the HD-VSFG spectra measured in SSP and PPP only depend on the frequency dependence of the hyperpolarizability elements and the orientational parameter D.

The HD-VSFG signal of the symmetric and the asymmetric vibration of the methyl group show a different dependence on the orientational factor D. Both vibrations are observed in the HD-VSFG spectrum measured in PPP polarization configuration. Hence, this spectrum can be used to determine D. For R (=β_{aac}/β_{ccc}) of ethanol a value of 3.4, and for β_{ccc}/β_{aca} of ethanol, a value of 0.22 has been reported.[48] In order to fit the data, the Fresnel coefficients L_{ii} introduced in equations (1) and (2) are required. The Fresnel factors depend on the refractive indices of the samples and on the refractive index of interfacial layer. To obtain these, literature values for ethanol/H_2O mixtures were interpolated and adapted for the concentrations investigated.[49] To obtain an estimate of the refractive index of the interfacial layer, the approach of Shen et al.[27] was followed. Using these values, we fit the measured HD-VSFG spectra assuming Lorentzian functions for the frequency dependence of the symmetric and the asymmetric C-H stretch vibrations of the methyl group (see SI). We thus obtain the orientational parameter D as a function of the mole percentage of ethanol. The result is shown in Figure 9a.

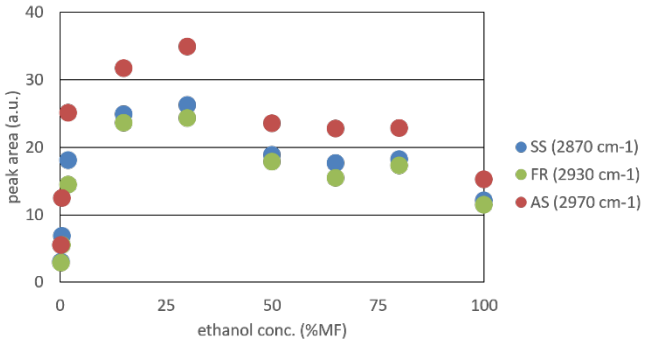

Figure 8: Peak areas of the fitted CH resonances detected in the PPP spectra.

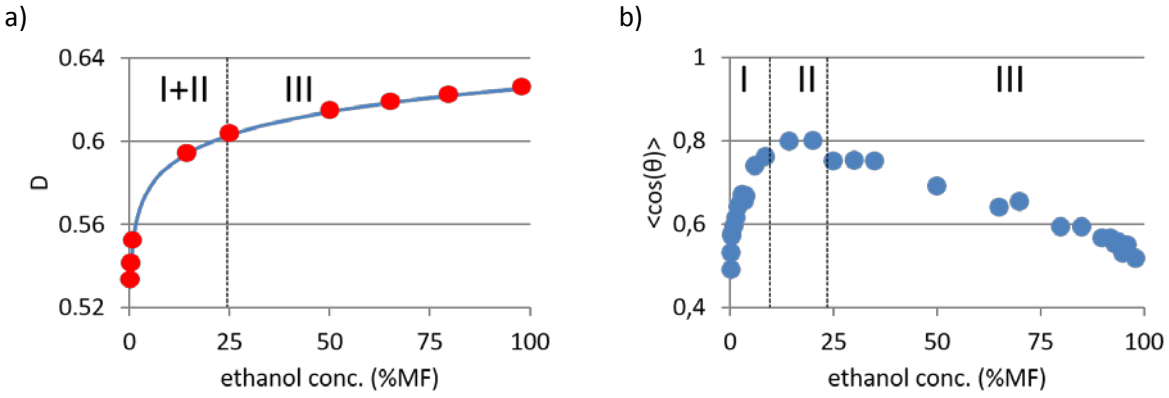

Figure 9: a) Dependence of the orientation parameter D and b) ⟨cos(θ)⟩ on the ethanol concentration. The red data points in a) were determined from the heterodyne detected SFG spectra using the strategy described in the text. The values of D at the other ethanol concentrations were obtained by interpolation of the red data points. With these D values, the values of ⟨cos(θ)⟩ at the corresponding ethanol concentrations were obtained by fitting the SFG intensity spectra in SSP polarization. The three Roman numbers I, II, and III indicate different concentration regions. To obtain an estimate of the fit quality, an exemplary fit of a spectrum is shown in the SI.

Determination of ⟨cos(θ)⟩

The signal measured with VSFG for different vibrations and for different polarization configurations is given by equations (4)-(9). In the previous subsection, the values of *D* at different ethanol molar fractions were determined, using the results of HD-VSFG measurement and literature values for the hyperpolarizabilities. The only unknown parameters of equations (4)-(9) are thus the surface number density N_S of ethanol molecules, and the average orientation ⟨cos(θ)⟩ of the molecules at the surface. By taking the surface number density N_S probed with VSFG proportional to the surface number density measured with PES (the signal indicated with 'PES surface' in Figure 6), we can determine the dependence of ⟨cos(θ)⟩ on the ethanol molar fraction from the intensity VSFG spectra. The corrected ethanol surface density ($N_{S,max}$ in eq. (3)) represents the surface-specific contribution of the PES signal. The good agreement of the disappearance of the free OH peak and the increase of the C1s peaks in the PES data indicates that the bulk contribution corrected PES data reflect the highly specific molecular-scale surface density of ethanol. It is assumed that this top layer of ethanol shows a non-symmetric orientation with the hydrophobic ethyl tail pointing outward. It should also be noted that we can only determine the relative change of ⟨cos(θ)⟩ upon a variation of the concentration of ethanol. The VSFG measurements in the free OH region indicate a complete surface coverage around 15% MF, and thus we assume that at this concentration the surface consists of a tightly packed ethanol surface layer. We take the value of ⟨cos(θ)⟩ to be equal to 0.8 at 15% MF, which corresponds to an angle of ~35°. This angle corresponds to the average orientation angle of alkyl chains in a well-packed surface layer.[50,51] The disappearance of the free OH peak at MF = 0.15 (see Figure 3 b)) indicates that at this mole fraction the top layer is fully covered by ethanol molecules, suggesting such a well-packed layer. The choice of this value for ⟨cos(θ)⟩ and thus of the minimum orientation angle mainly affects the absolute values of the angles, so the qualitative description of the behaviour as a function of the ethanol concentration remains largely unaffected. In Figure 9b we present the resulting ⟨cos(θ)⟩ as a function of the ethanol molar fraction.

Surface orientation angle and width of the angular distribution

The values of *D* and ⟨cos(θ)⟩ represent information on the orientation of the ethanol molecules at the surface. It is instructive to translate values of *D* and ⟨cos(θ)⟩ to an average orientation angle ⟨θ⟩ and a width of the orientational distribution at different molar fractions. To this purpose we need to translate the experimentally observed *D* and ⟨cos(θ)⟩ to an orientational probability distribution function *P*(θ). We assume *P*(θ) to be smooth, and to have an asymmetric shape given by a Gaussian multiplied by sin(θ):

$$P(\theta) = sin(\theta) e^{-(\theta-\theta_C)^2/2\sigma^2}, \; 0 < \theta < 180 \text{ degrees} \qquad (10)$$

where σ denotes the width of the angular distribution function, and θ_c is the central angle of this distribution function. The orientational distribution function *P*(θ) is proportional to sin(θ) which reflects the fact that for each polar angle θ there exists a circle of possible orientations (with different azimuthal space angle ϕ) of which the circumference depends on θ following sin(θ). This circumference and thus the probability goes to zero when θ goes to 0.
The value of ⟨cos(θ)⟩ is related to *P*(θ) following:

$$\langle cos(\theta) \rangle = \int_0^{\pi} cos(\theta) \; sin(\theta) e^{-(\theta-\theta_C)^2/2\sigma^2} \, d\theta \qquad (11)$$

and the orientational parameter *D*, is related to P(θ) according to:

$$D = \frac{\int_{0°}^{180°} cos^3(\theta) \, sin(\theta) \, e^{-(\theta-\theta_C)^2/2\sigma^2} \, d\theta}{\int_{0°}^{180°} cos(\theta) \, sin(\theta) \, e^{-(\theta-\theta_C)^2/2\sigma^2} \, d\theta} \qquad (12)$$

In the Supplementary information we present contour plots of ⟨cos(θ)⟩ and *D* as a function of the central angle θ_c and the

width σ of $P(\theta)$. Vice versa, we can use the experimentally determined values of $\langle\cos(\theta)\rangle$ and D to determine the values of θ_c and the width σ of the orientational distribution function $P(\theta)$. This $P(\theta)$ directly yields the average orientation angle $\langle\theta\rangle = \int d\theta\, P(\theta)\, \theta$, and the width of the orientational distribution, as defined as the full-width-at-half-maximum of $P(\theta)$. In Figure 10 we present $\langle\theta\rangle$ and the FWHM of the orientational distribution as a function of the molar fraction of ethanol. It should be noted that these parameters will be dependent on the chosen functional form of $P(\theta)$, i.e. if $P(\theta)$ would consist of several peaks (representing specific preferred orientations), the $\langle\theta\rangle$ and FWHM of $P(\theta)$ derived from $\langle\cos(\theta)\rangle$ and D would be different. Such a peaked orientational distribution would potentially represent a bilayer of ethanol molecules at the surface of the mixture. However, in view of molecular dynamics simulation results it seems unlikely that $P(\theta)$ would be highly structured. In fact, the obtained shapes are quite similar to the functional form of equation (10).[18]

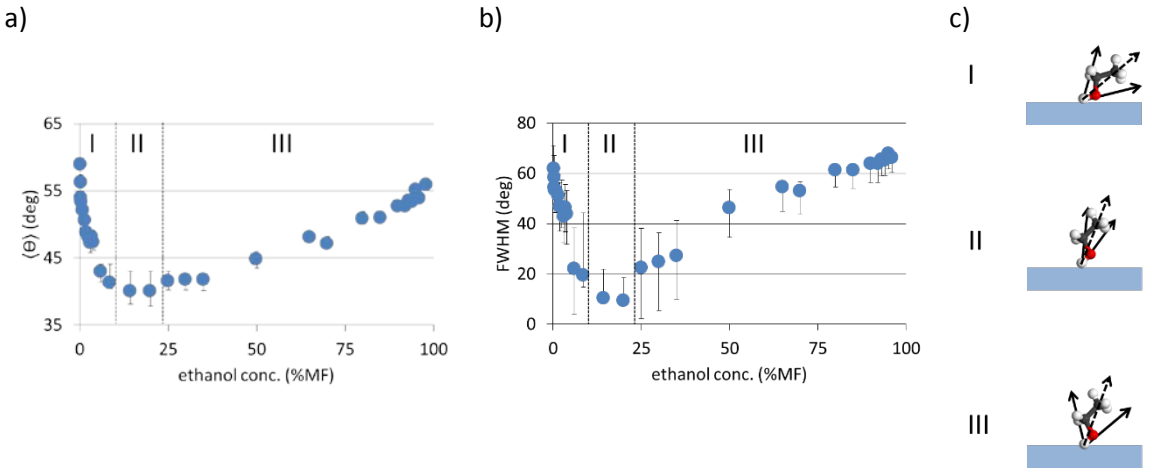

Figure 10: a) The average polar orientation angle $\langle\theta\rangle$ and b) full-width-at-half-maximum of the orientational distribution as a function the molar fraction of ethanol. The obtained values are calculated from the experimentally determined orientational parameters D and $\langle\cos(\theta)\rangle$ using an orientational distribution function $P(\theta)$ defined in the text. The error bars were calculated using a variation from the fitted result of D of ±0.05 (see Suppl. Information). Panel c) shows a schematic representation of the resulting fitted orientation and width of the angular distribution in the three different concentration regions that were defined in Figure 9b.

It follows from Figure 10 that the average orientation angle of the ethanol molecules and the FWHM of the orientational distribution vary substantially as a function of the molar fraction of ethanol. We distinguish three concentration ranges. In the low concentration region I (as defined in Figure 10), the average orientation angle $\langle\theta\rangle$ strongly decreases with increasing concentration of ethanol molecules, from ~60 degrees at MF=0 to ~40 degrees at MF=0.1. In this MF interval, the FWHM of the orientational distribution also strongly decreases. This latter trend shows that the ethanol molecules become increasingly ordered at the surface up to MF=0.1. Between MF=0.1 and MF=0.2, the average angle $\langle\theta\rangle$ remains ~40 degrees and the FWHM of the orientational distribution retains its minimum value (region II). As the concentration further increases (region III), both the average angle $\langle\theta\rangle$ and the FWHM of the orientational distribution gradually increase, reflecting an increasing disorder of the top molecular layers of the ethanol-water mixture. This randomization of the orientation of the ethanol molecules (in particular the increase of the tilt angle) explains the decrease of the VSFG signal of water-ethanol mixtures at high concentrations. The behaviour could be due to a transition from a monolayer of ethanol molecules of which the hydroxyl groups are strongly solvated by water underneath which results in a well-defined orientation, to a hydrogen-bonded network of primarily ethanol molecules at the surface, resulting in a loss of this orientational order. This interpretation is in accordance with MD simulations.[18]

Discussion

In several previous studies of mixtures of water and alcohols it has been found that the VSFG intensity of the alcohol C-H stretch vibrations reaches a maximum at an intermediate composition. This observation has been explained in different ways.[15–22] In the study by Chen et al.[19] of methanol-water mixtures, the occurrence of a maximum of the VSFG intensity signal at intermediate alcohol concentrations was explained from the formation of a second layer of methanol molecules underneath the surface. In this second layer the molecules would have an anti-parallel orientation to the top surface layer, and as a result the VSFG signal of these methanol molecules would destructively interfere with the signal coming from the top surface, thus explaining the decrease of the overall observed VSFG signal at high alcohol concentrations. However, the formation of such a second layer with an anti-parallel orientation of the methanol molecules is not supported by molecular dynamics simulations of methanol-water mixtures.[18]

The maximum in the intensity VSFG signal at intermediate compositions of water-alcohol mixtures has also been explained from a lowering of the surface density of alcohol molecules when the alcohol concentration is increased beyond

a certain MF.[16,17] This interpretation was based on the fact that the orientation of the alcohol molecules was believed not to change with alcohol concentration. However, this latter conclusion followed from a study of the orientation of the alcohol molecules at the surface that was based on the comparison of the VSFG intensity signal of the symmetric CH_3 vibration measured in SSP and in PPP polarization configurations. This means that the information on the orientation was derived from intensity VSFG signals measured in two different experiments. It is clear from the HD-VSFG spectra shown in Figure 7 that the sign of Im $\chi^{(2)}$ of the symmetric CH_3 vibration changes when going from SSP to PPP. As a consequence, the interference with the non-resonant background and other nearby vibrational resonances will change substantially going from SSP to PPP, which strongly affects the measured total VSFG intensity at the frequency of the symmetric CH_3 stretch. This change in interference complicates the determination of the orientation of the alcohol molecules at the surface from the ratio of the VSFG intensity signals measured with SSP and PPP polarization configurations. Moreover, in a recent combined intensity VSFG and molecular dynamics study of mixtures of water and methanol by Ishihara et al.[18] it was shown that the ratio of the intensity VSFG signals obtained with SSP and PPP is quite insensitive to changes in the orientational distribution of the methanol molecules at the surface. The MD simulations in this work showed that the average orientation changes quite strongly going from a methanol MF of 0.1 to bulk methanol ($\langle\cos(\theta)\rangle$ decreasing by a factor of 2), and that this change in orientation hardly affects the ratio of the intensity VSFG signals measured in SSP and PPP.

Li et al. observed a maximum in the SFG intensity as a function of the methanol fraction, which is attributed to a decrease of the hyperpolarizability of methanol with increasing methanol mole fraction.[52] This latter interpretation is based on the observation that the Raman intensity of the CH3-ss mode shows a nonlinear dependence on the methanol mole fraction. Based on MD simulations it was argued, that the surface density NS times $\langle\cos(\theta)\rangle$ (with θ the angle with the surface normal) would not show a maximum at an intermediate methanol mole fraction.[52] However, in the comment by Ishiyama it is shown that the presumed decrease of the hyperpolarizability is not present. The observed deviation from linearity of the Raman intensity of the CH3-ss mode on the methanol mole fraction can be nearly completely explained from the (nonlinear) dependence of the number density of methanol molecules on the methanol mole fraction.[53] In addition, in this comment it was shown that NS $\langle\cos(\theta)\rangle$ likely shows a maximum at a methanol mole fraction of ~0.7, due to an increasing disorder in the orientation of the methanol molecules at the surface.[53]

In this work we have studied the orientation of the ethanol molecules by comparing the amplitudes of the signals of the symmetric and the asymmetric CH_3 vibration measured with heterodyne-detected VSFG in PPP polarization configuration, and we find strong evidence that the average orientation of the alcohol molecules does change with increasing MF. The findings of the present HD-VSFG measurements of ethanol-water mixtures agree well with the results of the work of Ishihara et al.[18], and constitute the first experimental evidence that the orientational distribution of ethanol molecules at the surface changes quite strongly when the ethanol MF is varied from MF=0.1 to bulk ethanol. At the same time, the PES results show that the surface density of ethanol molecules is more or less constant in this concentration range. Hence, we can conclude that the observed maximum of the VSFG signal at MF=0.1 results from that the maximum surface density is attained at this composition, and that further increasing the ethanol concentration increases the orientational disorder at the surface.

It is also interesting to note that at about 20% MF of ethanol concentration both the average polar orientation and the FWHM of the orientational distribution show a minimum, see Figure 10 a and b. A possible explanation is that at this mole fraction a well-packed single molecular layer of ethanol molecules is established at the surface of a water-dominated solution. At lower mole fractions, the coverage of the surface is not yet complete leading to a larger orientational freedom of the ethyl groups of the ethanol molecules, while at higher mole fractions several layers of ethanol start to accumulate leading to a less strong average orientation of the ethanol molecules. This minimum coincides with a dip in the differential CH3 - CH2 C1s chemical shift at 20% MF predicted by quantum mechanics - molecular mechanics calculations averaged over trajectories from MD simulations.[54] This dip was later confirmed by the XPS measurements of Marinho et al.[46] The dip was further analysed in terms of a change of the H-bond configurations as a function of the ethanol concentration, and this analysis indicated a shift from a dominance of 3 H-bond to 2 H-bond configurations among the sampled structures.[54] Unfortunately, the statistical uncertainty of both the differential shifts and the H-bond distributions precluded a more definite conclusion about the structural changes occurring near an ethanol concentration of 20% MF.

Conclusions

We have studied the surface properties of binary ethanol-water mixtures over a broad composition range with vibrational surface sum-frequency generation spectroscopy (VSFG) and photoelectron spectroscopy (PES). We observe that the addition of ethanol to water leads to a strong non-linear increase of the surface concentration of ethanol up to an ethanol MF of ~0.1. This increase in surface concentration is reflected in the rapid increases of the C1s signal measured with PES, the decrease of the VSFG signal of the dangling OH vibrations of water molecules at the surface, and the increase of the VSFG signal of the methyl stretch vibrations of ethanol.

When the ethanol molar fraction is increased above 0.1, the total PES signal keeps rising as a result of an increasing bulk contribution. However, from a decomposition of the PES signal in a surface and a bulk contribution, we find that this increase

is due to an increase of the bulk contribution to the PES signal and that the surface concentration of ethanol remains constant for MF>0.1. The VSFG signal of the methyl vibrations of ethanol starts to decrease for ethanol MF>0.1, which indicates that the ethanol molecules at the surface become increasingly disordered.

We furthermore studied the orientation of the ethanol molecules at the surface with heterodyne detected VSFG measurements. With this technique we determined the orientational parameter D (= $\langle\cos^3\theta\rangle/\langle\cos\theta\rangle$), with θ the angle between the C-C bond of the ethanol molecule and the surface normal. Combination of these results with the VSFG intensity measurements and the PES data allows us to quantify θ and the FWHM of the orientational distribution at all ethanol concentrations. At low ethanol concentrations (region I) the tilt angle θ is ~60 degrees and the FWHM of the orientational distribution is ~60 degrees. When the ethanol concentration is increased to MF=0.1, the tilt angle decreases to ~40 degrees, and the FWHM to ~20 degrees, showing that the ethanol molecules form a well-ordered complete monolayer at MF=0.1. This orientational distribution persists up to MF=0.2 (region II). When the ethanol concentration of the ethanol-water mixture is further increased towards bulk ethanol, the tilt angle θ gradually increases to 55 degrees and the FWHM of the orientational distribution to 70 degrees.

Conflicts of interest

There are no conflicts to declare.

[1] P. Jungwirth, B.J. Finlayson-Pitts, and D.J. Tobias, Chem. Rev. **106**, 1137 (2006).
[2] H.-F. Wang, W. Gan, R. Lu, Y. Rao, and B.-H. Wu, Int. Rev. Phys. Chem. **24**, 191 (2005).
[3] A.G. Lambert, P.B. Davies, and D.J. Neivandt, Appl. Spectrosc. Rev. **40**, 103 (2005).
[4] Y.R. Shen, Annu. Rev. Phys. Chem. **64**, 129 (2013).
[5] G.L. Richmond, Chem. Rev. **102**, 2693 (2002).
[6] L. Zhang, W. Liu, Y.R. Shen, and D.G. Cahill, J. Phys. Chem. C **111**, 2069 (2007).
[7] W.T. Liu, L. Zhang, and Y.R. Shen, J. Chem. Phys. **125**, (2006).
[8] J.H. Guo, Y. Luo, A. Augustsson, S. Kashtanov, J.E. Rubensson, D.K. Shuh, H. Ågren, and J. Nordgren, Phys. Rev. Lett. **91**, 1 (2003).
[9] S. Dixit, J. Crain, W.C.K. Poon, J.L. Finney, and A.K. Soper, Nature **416**, 829 (2002).
[10] R.K. Lam, J.W. Smith, and R.J. Saykally, J. Chem. Phys. **144**, (2016).
[11] T. Takamuku, K. Saisho, S. Nozawa, and T. Yamaguchi, J. Mol. Liq. **119**, 133 (2005).
[12] M. Tarek, D.J. Tobias, and M.L. Klein, J. Chem. Soc. Trans. **92**, 559 (1996).
[13] E. Stewart, R.L. Shields, and R.S. Taylor, J. Phys. Chem. B **107**, 2333 (2003).
[14] M.A. Wilson and A. Pohorille, J. Phys. Chem. B **101**, 3130 (1997).
[15] N. Atamas and A. Atamas, World Acad. Sci. Eng. Technol. **55**, 1 (2009).
[16] J. Sung, K. Park, and D. Kim, JKPS **44**, 1394 (2004).
[17] J. Sung, K. Park, and D. Kim, J. Phys. Chem. B **109**, 18507 (2005).
[18] T. Ishihara, T. Ishiyama, and A. Morita, J. Phys. Chem. C **119**, 9879 (2015).
[19] H. Chen, W. Gan, B.H. Wu, D. Wu, Y. Guo, and H.F. Wang, J. Phys. Chem. B **109**, 8064 (2005).
[20] K. Wolfrum, H. Graener, and A. Laubereau, Chem. Phys. Lett. **213**, 41 (1993).
[21] J.Y. Huang and M.H. Wu, Phys. Rev. E **50**, 3737 (1994).
[22] G. Ma and H.C. Allen, J. Phys. Chem. B **107**, 6343 (2003).
[23] S. Strazdaite, J. Versluis, E.H.G. Backus, and H.J. Bakker, J. Chem. Phys. **140**, (2014).
[24] S. Strazdaite, J. Versluis, and H.J. Bakker, J. Chem. Phys. **143**, (2015).
[25] P.B. Miranda and Y.R. Shen, J. Phys. Chem. B **103**, 3292 (1999).
[26] R. Lu, W. Gan, B.H. Wu, H. Chen, and H.F. Wang, J. Phys. Chem. B **108**, 7297 (2004).
[27] X. Zhuang, P. Miranda, D. Kim, and Y. Shen, Phys. Rev. B **59**, 12632 (1999).
[28] M. Bässler, J.-. O. Forsell, O. Björneholm, R. Feifel, M. Jurvansuu, S. Aksela, S. Sundin, S.L. Sorensen, R. Nyholm, A. Ausmees, and S. Svensson, J. Electron Spectros. Relat. Phenomena **101–103**, 953 (1999).
[29] M. Bässler, A. Ausmees, M. Jurvansuu, R. Feifel, J.O. Forsell, P. De Tarso Fonseca, A. Kivimäki, S. Sundin, S.L. Sorensen, R. Nyholm, O. Björneholm, S. Aksela, and S. Svensson, Nucl. Instruments Methods Phys. Res. Sect. A Accel. Spectrometers, Detect. Assoc. Equip. **469**, 382 (2001).
[30] S. Thürmer, R. Seidel, M. Faubel, W. Eberhardt, J.C. Hemminger, S.E. Bradforth, and B. Winter, Phys. Rev. Lett. **111**, 1 (2013).
[31] N. Ottosson, M. Faubel, S.E. Bradforth, P. Jungwirth, and B. Winter, J. Electron Spectros. Relat. Phenomena **177**, 60 (2010).
[32] H.T. Nguyen-Truong, J. Phys. Condens. Matter **30**, (2018).
[33] B. Winter, Nucl. Instruments Methods Phys. Res. Sect. A Accel. Spectrometers, Detect. Assoc. Equip. **601**, 139 (2009).
[34] R. Seidel, S. Thürmer, and B. Winter, J. Phys. Chem. Lett. **2**, 633 (2011).
[35] M. Faubel and B. Winter, ChemInform **37**, 1176 (2006).
[36] H. Bergersen, R.R.T. Marinho, W. Pokapanich, A. Lindblad, O. Björneholm, L.J. Sæthre, and G. Öhrwall, J. Phys. Condens. Matter **19**, (2007).
[37] S. Hüfner, *Photoelectron Spectroscopy*, 3. edition (Springer Verlag Berlin Heidelberg, Berlin, 2003).
[38] B. Winter, R. Weber, W. Widdra, M. Dittmar, M. Faubel, and I. V. Hertel, J. Phys. Chem. A **108**, 2625 (2004).
[39] J.L. Campbell and T. Papp, At. Data Nucl. Data Tables **77**, 1 (2001).
[40] E.A. Raymond, T.L. Tarbuck, M.G. Brown, and G.L. Richmond, J. Phys. Chem. B **107**, 546 (2003).
[41] A. Chodzińska, A. Zdziennicka, and B. Jańczuk, J. Solution Chem. **41**, 2226 (2012).
[42] G. Vazquez, E. Alvarez, and J.M. Navaza, J. Chem. Eng. Data **40**, 611 (1995).
[43] R. Lu, W. Gan, B.H. Wu, Z. Zhang, Y. Guo, and H.F. Wang, J. Phys. Chem. B **109**, 14118 (2005).
[44] W. Gan, B. Wu, Z. Zhang, Y. Guo, and H. Wang, J. Phys. Chem. C **111**, 8716 (2007).
[45] M. Abu-Samha, K.J. Børve, L.J. Sæthre, and T.D. Thomas, Phys. Rev. Lett. **95**, 2 (2005).

[46] R.R.T. Marinho, M.-M. Walz, V. Ekholm, G. Öhrwall, O. Björneholm, and A.N. de Brito, J. Phys. Chem. B **121**, 7916 (2017).
[47] S. Strazdaite, J. Versluis, N. Ottosson, and H.J. Bakker, J. Phys. Chem. C **121**, 23398 (2017).
[48] H. Wu, W.-K. Zhang, W. Gan, Z.-F. Cui, and H.-F. Wang, J. Chem. Phys. **125**, 133203 (2006).
[49] R.J. Jiménez Riobóo, M. Philipp, M.A. Ramos, and J.K. Krüger, Eur. Phys. J. E **30**, 19 (2009).
[50] W. Liu, L. Zhang, and Y.R. Shen, Chem. Phys. Lett. **412**, 206 (2005).
[51] H. Xu, D. Zhang, J. Hu, C. Tian, and Y.R. Shen, J. Phys. Chem. A **119**, 4573 (2015).
[52] X. Li, J. Liu, K. Lin, Y. Zhang, Y. Zhang, R. Zheng, Q. Shi, Y. Guo, and Z. Lu, J. Phys. Chem. C **123**, 12975 (2019).
[53] T. Ishiyama, S. Takagi, T. Hirano, L. Wang, and A. Morita, J. Phys. Chem. C **124**, 25160 (2020).
[54] T. Löytynoja, J. Niskanen, K. Jänkälä, O. Vahtras, Z. Rinkevicius, and H. Ågren, J. Phys. Chem. B **118**, 13217 (2014).

